OPEN ACCESS

Original research

Hybrid identity and distinct methylation profiles of incomplete intestinal metaplasia in the stomach

Hyesung Kim,[1] Junseong Kim,[2] In Ho Jeong,[3,4] Eunsun Park,[5] Mira Yoo,[5] Seokho Yoon,[5] Donghyun Lee,[3,4] Jaekyung Myung,[6,7] Eunyoung Choi ,[8,9,10] James R Goldenring ,[8,9,10,11] Bogun Jang [5,12]

► Additional supplemental material is published online only. To view, please visit the journal online (https://doi.org/10.1136/gutjnl-2025-335793).

For numbered affiliations see end of article.

Correspondence to
Dr Bogun Jang;
bgjang9633@gmail.com

Received 5 May 2025
Accepted 4 July 2025

ABSTRACT

Background Gastric intestinal metaplasia (GIM), particularly the incomplete subtype (Inc IM), is strongly associated with increased gastric cancer (GC) risk. However, its role as a true precursor lesion remains uncertain.

Objective We aimed to delineate the molecular identity, differentiation potential and oncogenic relevance of Inc IM.

Methods Spatial transcriptomics using a custom lineage-enriched panel was applied to profile GIM and GC tissues. Subtype-specific GIM organoid models were developed for DNA methylation and chromatin accessibility profiling. Single-cell RNA sequencing was performed to evaluate differentiation capacity.

Results Spatial transcriptomics revealed that Inc IM potentially originates from the deep antral gland cells and harbours a hybrid transcriptomic signature incorporating gastric, small intestinal and large intestinal lineages across both differentiated and stem/progenitor compartments. DNA methylation profiling of subtype-specific organoids showed that Inc IM exhibits extensive intergenic hypermethylation, resembling native antral mucosa. In contrast, complete subtype was marked by promoter hypermethylation of tumour suppressor genes and displayed a more fully intestinalised epigenetic profile. Organoid models recapitulated subtype-specific traits and demonstrated lineage plasticity. Spatial mapping of GC samples revealed an enrichment of Inc IM-like cells, particularly within microsatellite stable tumours. Approximately 76% of the GCs analysed were linked to GIM, while the remaining (24%) appeared to be associated with deep antral differentiation.

Conclusions Inc IM represents a phenotypically unstable and epigenetically deregulated metaplastic state with dual-lineage potential and molecular resemblance to GC. These findings establish Inc IM as a true precursor to GC and underscore the importance of active surveillance and early intervention strategies.

WHAT IS ALREADY KNOWN ON THIS TOPIC

⇒ Incomplete-type gastric intestinal metaplasia (GIM) (Inc IM) is associated with a higher risk of gastric cancer (GC) development based on epidemiologic studies. However, its cellular and molecular identities, as well as molecular evidence linking it to GC, remain poorly defined.

WHAT THIS STUDY ADDS

⇒ Spatial transcriptomic profiling revealed that Inc IM potentially arises from the antral basal gland cells and displays a unique hybrid gastric–intestinal transcriptional signature spanning both differentiated and stem/progenitor cell compartments. Inc IM organoids recapitulated this dual identity and exhibited bipotent differentiation on bone morphogenic protein stimulation. Epigenetically, Inc IM exhibited widespread intergenic hypermethylation with a methylation landscape more closely resembling native antral mucosa. In contrast, complete IM was characterised by promoter hypermethylation of tumour suppressor genes and a more fully intestinalised epigenetic profile. In addition, spatial mapping identified Inc IM-like cells in a subset of GCs, particularly microsatellite stable subtype, indicating a phenotypic continuum from Inc IM to GC. Approximately 76% of GCs are associated with GIM, while the remaining GCs (24%) were linked to deep antral differentiation.

HOW THIS STUDY MIGHT AFFECT RESEARCH, PRACTICE OR POLICY

⇒ By identifying Inc IM as a higher-risk precancerous lesion, our findings underscore the need for risk stratification based on its extent, with potential implications for surveillance and early intervention strategies.

Check for updates

To cite: Kim H, Kim J, Jeong IH, *et al*. *Gut* Epub ahead of print: [*please include* Day Month Year]. doi:10.1136/gutjnl-2025-335793

INTRODUCTION

Gastric intestinal metaplasia (GIM) refers to the transformation of gastric epithelium into an intestinal phenotype, primarily driven by chronic inflammation caused by *Helicobacter pylori* (HP) infection.[1 2] GIM is widely recognised as a precancerous lesion that significantly increases the risk of developing intestinal-type gastric cancer (GC).[3] Histologically, GIM is categorised into two subtypes: complete intestinal metaplasia (Com IM) and incomplete IM (Inc IM).[4] These subtypes are traditionally distinguished by mucin expression profiles and morphological features, with Com IM resembling the small intestine (SI) and Inc IM resembling the colon.[5] However, accumulating evidence suggests that Inc IM may not entirely reflect a colonic phenotype. Rather, it appears to represent

a hybrid gastric-intestinal lineage.[6–8] Importantly, many epidemiological studies have consistently shown that Inc IM carries a substantially higher risk for GC development compared with Com IM.[9] Despite this clinical significance, relatively few studies have examined the molecular landscape of Inc IM in depth,[10–13] and none have specifically characterised the cellular phenotypes of Inc IM at single-cell resolution.

Murine models have demonstrated that oncogenic mutations in genes such as *Apc*, *Kras*, *p53*, *Smad* and *Cdh1* in gastric epithelial cells can lead to GC.[14] However, these models do not incorporate GIM as an intermediate step in Correa cascade, where intestinal-type GC typically arises through a sequence involving chronic gastritis, GIM, dysplasia and carcinoma. To date, no animal model has demonstrated that GC can arise directly from GIM stem cells. Transgenic mouse models expressing the intestine-specific homeobox genes *Cdx1* or *Cdx2* have demonstrated the development of classical GIM.[15 16] However, in these models, *Cdx1* or *Cdx2* expression was induced throughout the entire gastric epithelium, a condition that does not accurately reflect the nature of human GIM development. Furthermore, these models did not exhibit progression to GC. This gap has fuelled ongoing debate about whether GIM progresses to GC.[17]

In this study, we employed an integrative approach combining spatial transcriptomics, organoid modelling and single-cell RNA sequencing (scRNA-seq) to delineate the molecular features of Inc IM and its association with GC. Our findings reveal that Inc IM harbours a hybrid gastric-intestinal lineage identity across both superficial differentiated cells and stem/progenitor cell populations, underpinned by widespread DNA hypermethylation at intergenic regions. Importantly, we demonstrate a strong phenotypic and molecular continuity between Inc IM and GC, providing compelling evidence that Inc IM serves as a true precursor to GC. These results not only define the molecular identity of Inc IM but also underscore its clinical significance, advocating for active surveillance and early therapeutic intervention to mitigate GC risk.

METHODS

Detailed methods are provided in the online supplemental material.

Patient and public involvement

Patients and/or the public were not involved in the design, or conduct, or reporting, or dissemination plans of this research.

RESULTS

Spatially resolved transcriptomic analyses of GIM

To uncover the cellular and molecular phenotypes of GIM, we performed spatial transcriptomic analysis using the 10x Genomics Xenium platform with two tissue microarrays including samples of normal gastric mucosa, normal intestinal mucosa and GIM. The clinicopathological information of GC samples from which gastric tissues are derived is listed in online supplemental table 1. As the commercially available spatial transcriptomic panel lacks sufficient gene coverage to resolve the lineage and function of epithelial cells, we designed a custom panel comprising 293 genes enriched in epithelial cells from the stomach, SI and large intestine (LI) tissues (online supplemental table 2 and figure 1A). 29 cell clusters were initially identified, and epithelial clusters were reannotated into 21 clusters using histological evaluation and differential gene expression (DGE) profiling (online supplemental table 3). Our customised panel successfully resolved lineage-specific epithelial cell types across normal stomach, SI and LI tissues (figure 1B and online supplemental figure 1A,B). Com IM exhibited a cellular composition highly similar to that of normal SI, with only subtle differences in cell proportions, an expanded stem/progenitor population (figure 1B,C). An ambiguous lesion displaying features both Com and Inc IM, referred to as undetermined IM (Un IM), exhibited intestinal stem cell (ISC) clusters localised at the gland base, similar to SI and Com IM, but with distinct progenitor and surface cell populations (figure 1B,C). In contrast, Inc IM presented with a unique cellular architecture composed of distinct clusters annotated as Inc IM progenitor, Inc IM intermediate and Inc IM surface 1–3, while its basal gland regions resembled the antral glands (figure 1B,C and online supplemental figure 1B). Lineage-enriched gene expression analysis clearly demonstrated that Com IM closely resembled SI, while Inc IM exhibited a mixed expression profile incorporating markers from the stomach, SI and LI (figure 1D). Uniform Manifold Approximation and Projection (UMAP) further confirmed the intermediate state of Inc IM between gastric and intestinal lineages (figure 1E,F).

Early development of Inc IM within inflamed gastric mucosa

Notably, high-resolution spatial profiling enabled the identification of several discrete metaplastic foci within chronically inflamed gastric mucosa. One lesion located at the junction of the antral isthmus and basal gland regions was composed predominantly of Inc IM progenitor cells, indicative of early-stage Inc IM (figure 2A,B). A second lesion, also situated at a similar location, was enriched for intermediate enterocytes and intestinal progenitor cells, suggestive of early-stage Com IM (figure 2C,D). UMAP reveals that early Com IM, unlike Inc IM, appears disconnected from antral cells, suggesting a pronounced transition towards an intestinal phenotype in Com IM. Given that deep basal gland cells serve as stem cells in the human antrum,[18] these histo-spatial findings implicate that GIM originates from the basal gland stem cells and expands via progenitor cell proliferation at the isthmus. In another case, Com IM glands were embedded within Inc IM-dominant mucosa, populated primarily by ISC and progenitor cells with Inc IM progenitors interspersed throughout (figure 2E,F). This cellular arrangement raises the possibility of bidirectional plasticity or interconversion between Com IM and Inc IM stem/progenitor populations. Transcriptomic profiling of early Inc IM legion revealed upregulation of intestine-enriched genes such as *DMBT1*, *REG4*, *CDX2* and *REG1B* alongside downregulation of stomach-specific genes including *TFF2*, *CLU*, *AXIN2* and *GKN2* compared with adjacent gastric isthmus cells (figure 2H–J). Morphologically, the lesion appeared undifferentiated, with a thickened apical membrane (figure 2K). Among the highly upregulated genes, *DMBT1* was further validated at the protein level along with the proliferation and progenitor markers, STMN1 and Ki-67 (figure 2L), consistent with previous findings where DBMT1 was suggested as an early GIM marker since its expression precedes the appearance of typical GIM morphology.[19] To gain further insights into the developmental trajectory of GIM, we conducted trajectory and pseudotime analyses after excluding SI and LI samples from the cohort (figure 2M,O). These analyses revealed an overlapping region in which antral basal cells and Inc IM basal cell were closely located (figure 2M–O), suggesting that antral basal gland cells have the potential to give rise not only to gastric lineage cells but also to cells of the Inc IM lineage.

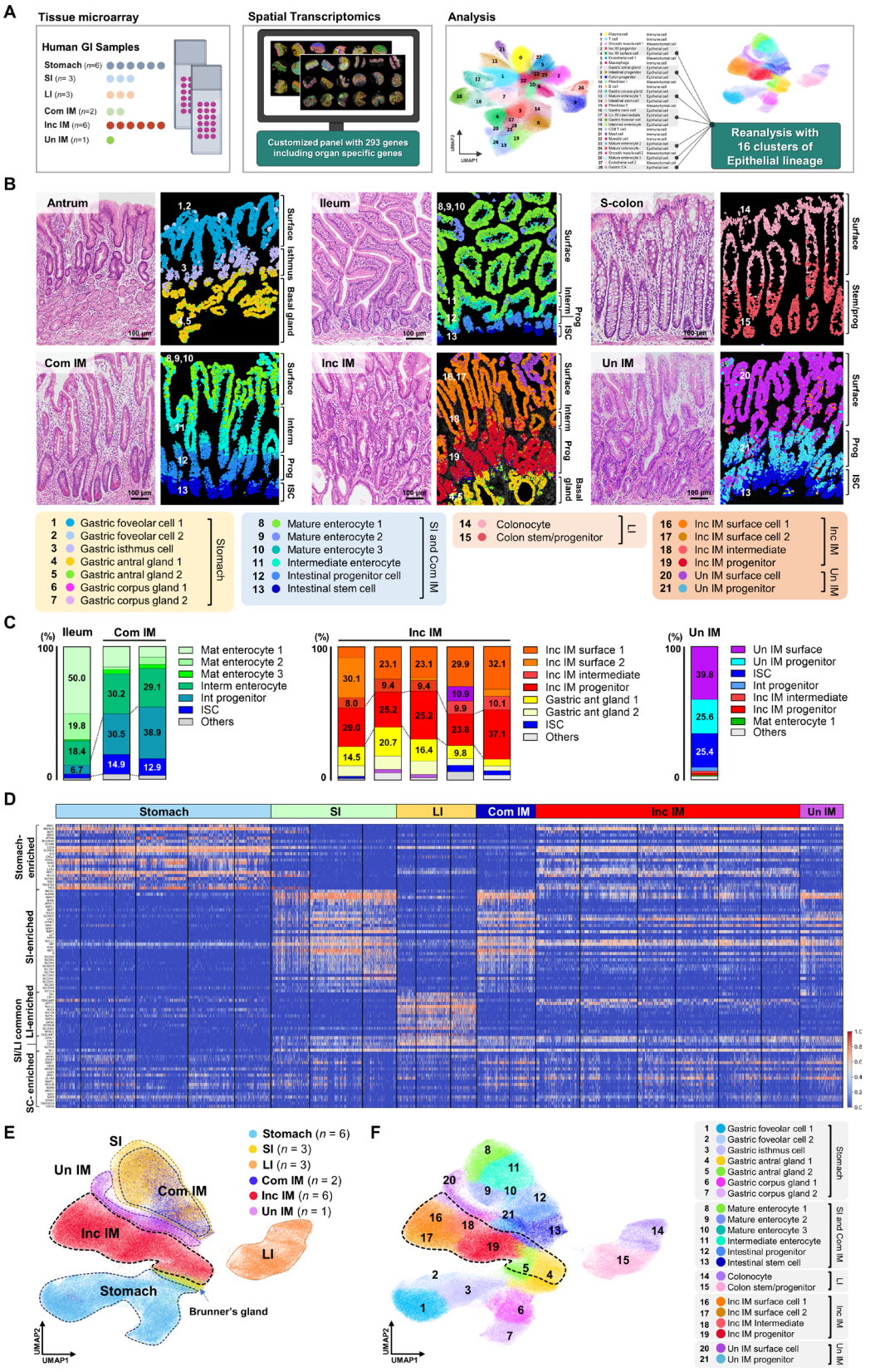

Figure 1 Spatially resolved transcriptomic analysis of gastric intestinal metaplasia (GIM). (A) Schematic overview of the spatial transcriptomic analysis workflow. Spatial transcriptomics was performed on tissue microarrays comprising human gastrointestinal samples using the Xenium platform (10x Genomics). (B) Representative H&E and corresponding Xenium images of antrum, ileum, sigmoid colon (S-colon) and GIM samples with cell type annotations. (C) Relative proportions of epithelial cell clusters. (D) Heatmap of organ-enriched and stem/progenitor cell-enriched genes across samples. (E) UMAP of epithelial cells from normal stomach, small intestine (SI), large intestine (LI) and GIM subtypes. (F) Cell type annotation of 21 epithelial cell clusters overlaid on UMAP. Com IM, complete intestinal metaplasia; Inc IM, incomplete subtype IM; ISC, intestinal stem cell; UMAP, Uniform Manifold Approximation and Projection; Un IM, undetermined IM.

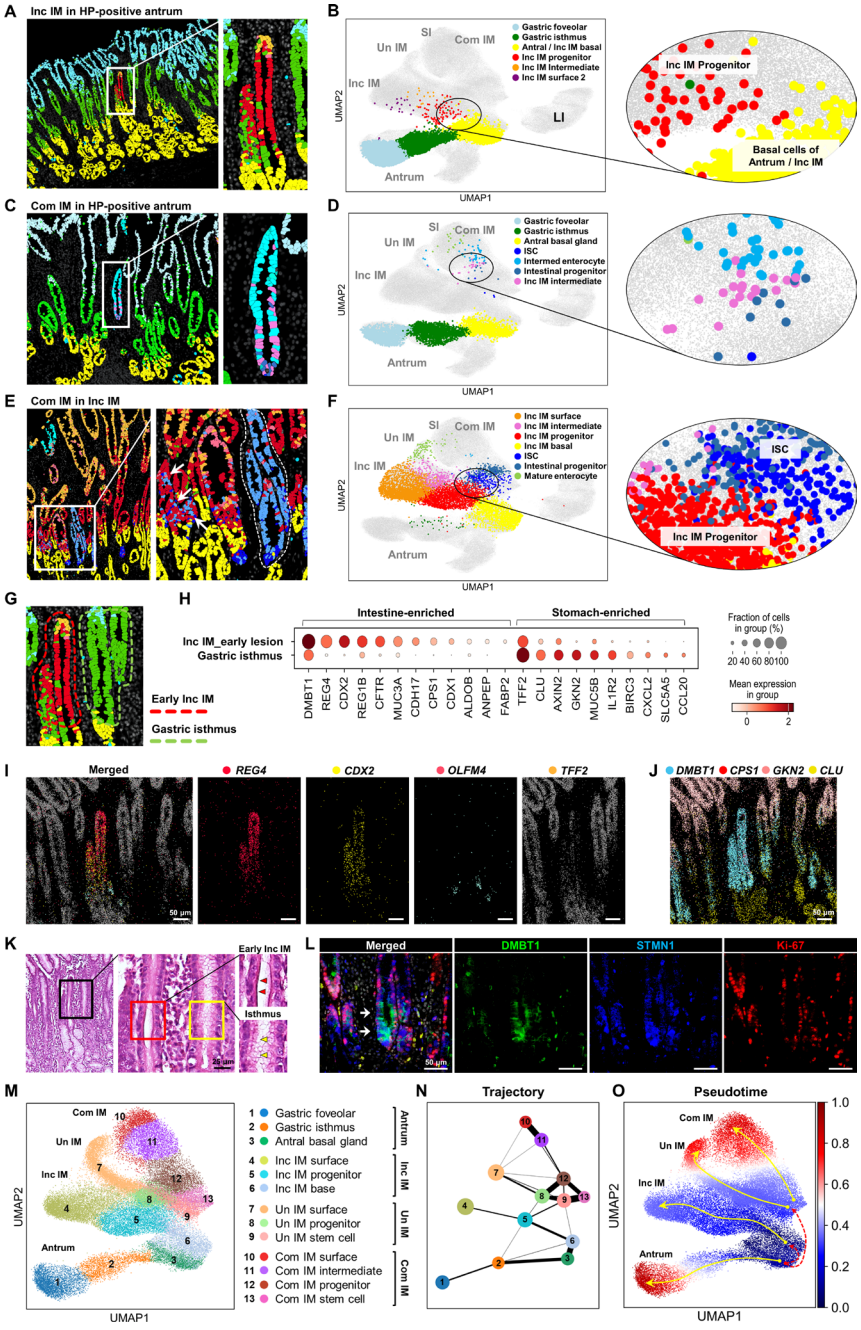

Figure 2 Identification of early gastric intestinal metaplasia (GIM) development within inflamed gastric mucosa. (A) Xenium image showing an early incomplete intestinal metaplasia (Inc IM) lesion localised to the neck region of *Helicobacter pylori*-positive inflamed gastric mucosa. The white boxed area is magnified on the right. (B) UMAP projection of cells from the tissue core containing the early Inc IM lesion overlaid onto the global UMAP of all samples. Cells from this specific core are displayed with increased dot size to enhance visibility. The black circled cluster is enlarged to highlight its distinct cellular composition. (C) Xenium image of an early complete IM (Com IM) gland within Helicobacter pylori-positive gastric mucosa. The white boxed area is enlarged on the right. (D) UMAP projection of cells from the tissue core including the early Com IM glands overlaid onto the global UMAP of all samples. (E) Xenium image showing early Com IM gland within an Inc IM-predominant mucosa. The white boxed region is magnified on the right; white arrows highlight intestinal stem cells (ISCs) and progenitors interspersed with Inc IM progenitors. (F) UMAP projection of cells from the tissue core including the early Com IM glands onto the global UMAP of all samples. ISCs of Com IM glands are observed in close proximity to Inc IM progenitor cells. (G, H) Differential gene expression analysis between early Inc IM cells (red dotted outline, cell number=173) and adjacent gastric neck cells (green dotted outline, cell number=203) in a Xenium image (G), showing distinct intestine- and stomach-enriched gene expression patterns (H). (I, J) Xenium images of early Inc IM glands showing expression of genes including *REG4, CDX2, OLFM4 and TFF2 (I), or DMBT1*, *CPS1*, *GKN2* and *CLU* (J). (K) H&E staining of early Inc IM lesion. The black boxed area is enlarged in the middle; red and yellow boxed regions are shown at higher magnification. Red arrowheads indicate metaplastic cells; yellow arrowheads indicate normal gastric neck cells. (L) Co-immunostaining of early Inc IM lesion with DMBT1, STMN1 and Ki-67. (M–O) UMAP (M), trajectory mapping (N) and Palantir pseudotime analysis (O) of normal antrum, Inc IM, Un IM and Com IM samples. Yellow arrows denote direction of differentiation of antral, Inc IM and Com IM lineages. Red dotted arrows represent the hypothetical direction of metaplastic transformation from the antral basal stem cell population. LI, large intestine; SI, small intestine; UMAP, Uniform Manifold Approximation and Projection.

Mixed lineage commitment of Inc IM

To dissect the lineage complexity of GIM, we focused on two major epithelial compartments: surface-differentiated cells and stem/progenitor cells. Morphologically, surface cells in Com IM closely resemble those of the SI, whereas surface cells in Inc IM and Un IM exhibit a heterogeneous phenotype with mixed features of stomach, SI and LI (figure 3A). UMAP demonstrated that surface epithelial cells from the stomach, SI and LI formed distinct clusters, with Com IM clustering primarily with SI, while Inc IM and Un IM were positioned between the stomach and SI clusters (figure 3B). DGE analysis supported this observation, revealing coexpression of lineage-specific markers from the stomach, SI and LI in Inc IM (figure 3C and online supplemental figure 2A). Feature plots of representative lineage markers highlighted the mixed identity of Inc IM surface cells (figure 3D). While Inc IM expressed fewer SI markers overall compared with Com IM, REG4 was more highly expressed in Inc IM than in Com IM (figure 3C and online supplemental figure 2A). This increased expression was due to REG4 being restricted to goblet cells in the SI and Com IM, whereas in Inc IM, it was broadly expressed across most surface cells (online supplemental figure 2B). Genes involved in digestion and metabolism were expressed at comparable levels in Com IM and Inc IM. However, genes responsible for nutrient transport were significantly lower in Inc IM (figure 3E and online supplemental figure 2C), indicating Inc IM represents a functionally immature intestinal phenotype. Representative Xenium images show surface cells in Inc IM co-expressing both gastric and intestinal markers (online supplemental figure 3A). This hybrid identity was further confirmed by co-immunostaining for CLDN18 and FABP2, showing clear colocalisation of gastric and intestinal markers at the cell surface (online supplemental figure 3B,C).

Given that metaplasia entails phenotypic reprogramming initiated from stem or progenitor cells that clonally remodel entire glandular units,[20] we next investigated the transcriptomic features of these cells (figure 3F). UMAP revealed a similar pattern to surface cells: Com IM clustered with SI, while Inc and Un IM localised between stomach and SI (figure 3G). Consistent with the findings from surface differentiated cells, stem/progenitor cells in Inc IM coexpressed markers from multiple lineages (figure 3H,I). These included the stomach-enriched transcription factor *SOX2*, the SI-associated markers *DMBT1* and *OLFM4*, and *LEFTY1*, a gene enriched in the LI (figure 3J). Representative Xenium images display stem/progenitor cells in Inc IM coexpressing multiple lineage markers (online supplemental figure 3D). *DMBT1* expression was validated at the protein level in both Com IM and Inc IM (online supplemental figure 3E). Interestingly, *LEFTY1* expression was observed specifically in LI and Inc IM stem/progenitor populations, but not in Com IM or normal gastric tissue (online supplemental figure 3F,G and table 4). Histologically, Inc IM retains deep antral-type gland cells in the basal compartment (online supplemental figure 4A). Although assigned to the same clusters and sharing specific gastric and stem cell markers (online supplemental figure 4B–D), basal Inc IM glands were distinct from antral glands on UMAP (online supplemental figure 4B) and were characterised by high expression of *OLFM4* and *LEFTY1*, and reduced expression of *TFF2* (online supplemental figure 4C–F), suggesting that they are more likely of Inc IM origin. Additionally, representative images illustrating the mixed-lineage phenotype of Inc IM are presented in online supplemental figure 5. In summary, our results reveal that Com IM is transcriptionally and phenotypically analogous to SI. In contrast, Inc IM harbours distinct epithelial populations with transcriptional profiles indicative of mixed gastric, SI and LI lineages, both in surface and stem/progenitor compartments.

Generation of subtype-specific GIM organoids and their epigenetic landscape

Metaplasia is believed to emerge through transcriptional reprogramming that alters cellular and lineage identity, a process largely orchestrated by epigenetic modifications. To elucidate the epigenetic landscape underpinning each GIM subtype, we first established gastric organoid lines from gastrectomy specimens (figure 4A). From these primary organoids, we selected three representative organoid types: organoids derived from antral mucosa without IM, Com IM-predominant mucosa and Inc IM-predominant mucosa (figure 4B and online supplemental figure 6A–C). To obtain subtype-specific organoid lines, single spheres were isolated from each pool and subjected to serial passaging (figure 4C and online supplemental figure 6D). At protein levels, SOX2 and CDX2 serve as lineage-specific markers for gastric and intestinal epithelium, respectively.[21] We confirmed their expression patterns in both tissue array samples (online supplemental figure 6E) and subtype-specific organoid lines (figure 4D). To further validate the lineage fidelity of each organoid type, we assessed the expression of stomach-enriched and intestine-enriched genes by RT-PCR before and after bone morphogenic protein (BMP) stimulation, a key regulator of gastrointestinal differentiation.[22] Notably, BMP-induced upregulation of *GKN1* and *GKN2* was the most consistent hallmark of non-metaplastic gastric organoids, with expression levels increasing by several hundred-fold to thousand-fold (figure 4E). Expression of *TFF2* and *SOX2* remained higher in antral organoids (online supplemental figure 6F). Among the intestinal markers, *ANPEP* and *ALDOB* were most prominently induced by BMP stimulation in Com IM organoids (figure 4E), while *CDX1*, *CDX2* and *REG4* were preferentially expressed in both Inc IM and Com IM (online supplemental figure 6F and table 5). Previously, we reported that combined treatment with a MEK inhibitor and Pyrvinium selectively induced cell death in dysplastic human gastric organoids while arresting the growth of non-dysplastic lines,[23] in which we did not discriminate GIM subtypes in non-dysplastic organoids. Here, we evaluated the same drug combination in Com IM and Inc IM organoids, observing comparable growth arrest or mild suppression in both GIM subtypes as well as in antral organoids (online supplemental figure 7A–D).

Next, we performed genome-wide DNA methylation profiling on organoids. Unsupervised hierarchical clustering demonstrated that Inc IM organoids aligned closely with antral organoids, while Com IM clustered with SI and LI counterparts (figure 4F). Inc IM organoids demonstrated extensive DNA hypermethylation, particularly in intergenic regions, a feature not observed in Com IM, which exhibited modest global methylation changes (figure 4G). Overall, Inc IM showed significantly higher DNA methylation levels than Com IM (online supplemental figure 8A), reaching levels comparable to those observed in SI and LI (online supplemental figure 8B–H). Locus-specific analysis further revealed that stomach-enriched loci such as *GKN2* and *CLDN18* remained hypomethylated in both the antrum and Inc IM (figure 4H and online supplemental figure 8I), while intestine-enriched loci including *OLFM4* and *FABP2* were hypermethylated in Inc IM but not in Com IM, SI or LI (figure 4I and online supplemental figure 8J). These patterns are consistent with transcriptomic findings and highlight the retained gastric identity of Inc IM despite its partial intestinalisation. We next examined the

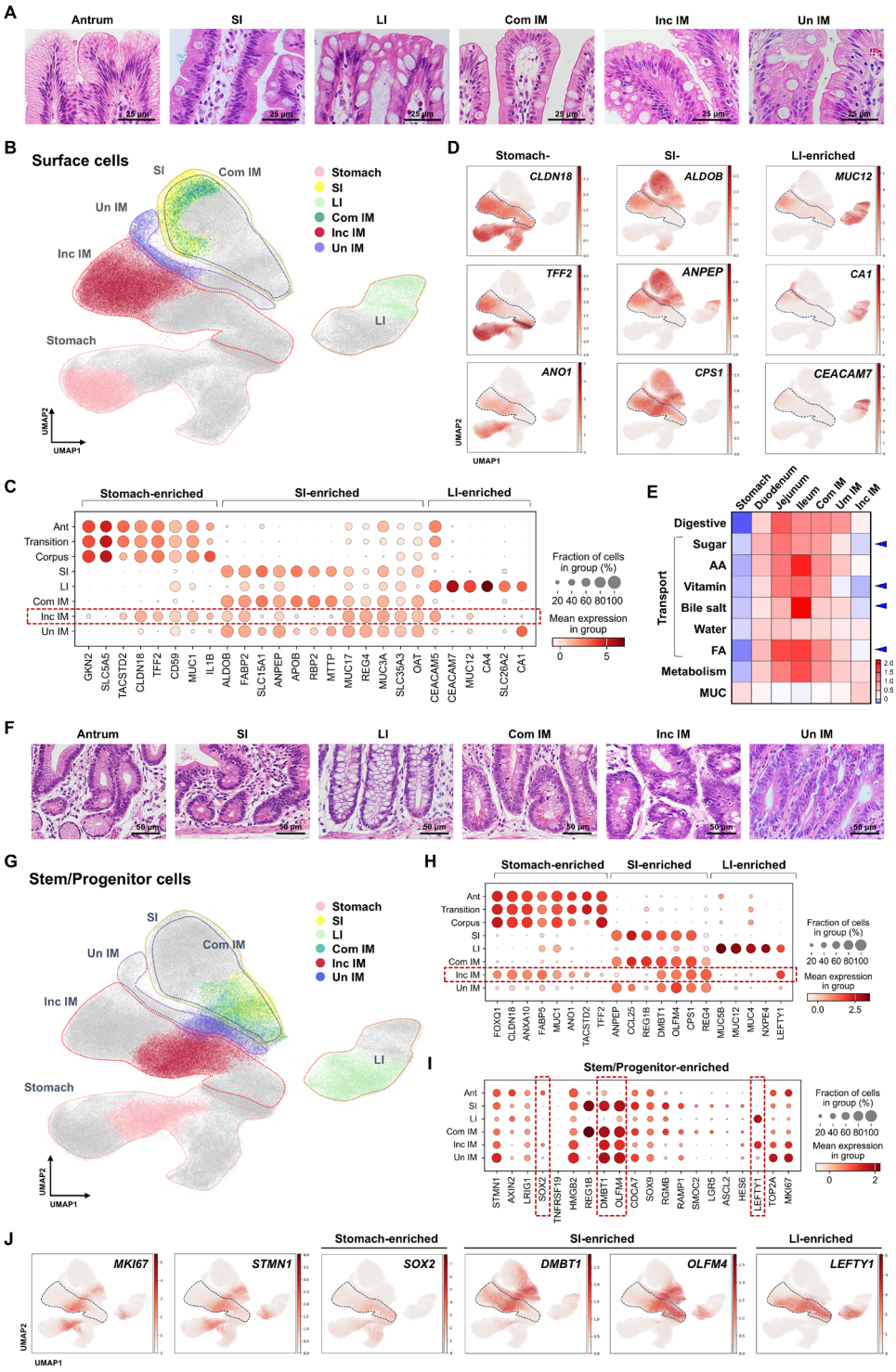

Figure 3 Mixed lineage identity of incomplete intestinal metaplasia (Inc IM). (A) Representative H&E images of the surface epithelial compartment in normal stomach and GIM tissues. (B) UMAP of surface epithelial cells derived from normal stomach, small intestine (SI), large intestine (LI) and GIM subtypes: complete (Com IM), Inc IM and undetermined (Un IM). (C) Dot plot showing differentially expressed genes in surface epithelial cells across normal and GIM tissues. Red dotted box highlights the mixed expression pattern of lineage-enriched genes in Inc IM. (D) Feature plots displaying the spatial expression of representative stomach, SI and LI marker genes. Inc IM is outlined with a black dotted line. (E) Heatmap summarising the mean expression levels of functionally annotated SI-enriched genes across SI regions and GIM subtypes. Blue arrowheads mark functional gene categories with low expression in Inc IM relative to SI and Com IM. (F) Representative H&E images showing the isthmus region of normal gastric mucosa and Inc IM, and the basal regions of SI, LI, Com IM and Un IM. (G) UMAP of stem/progenitor cell populations from normal stomach, SI, LI and GIM subtypes. (H) Dot plot of differentially expressed genes in stem/progenitor cell clusters from each tissue type. The red dotted box highlights the Inc IM cluster exhibiting co-expression of gastric and intestinal lineage markers. (I) Dot plot showing the expression of stem/progenitor cell-enriched genes across samples. Red dotted boxes indicate significant expression of lineage-enriched genes within Inc IM stem/progenitor cells. (J) Feature plots displaying spatial expression of *SOX2*, *DMBT1*, *OLFM4*, *LEFTY1* and proliferation-associated markers (*Ki-67* and *STMN1*) within the stem/progenitor compartment. UMAP, Uniform Manifold Approximation and Projection.

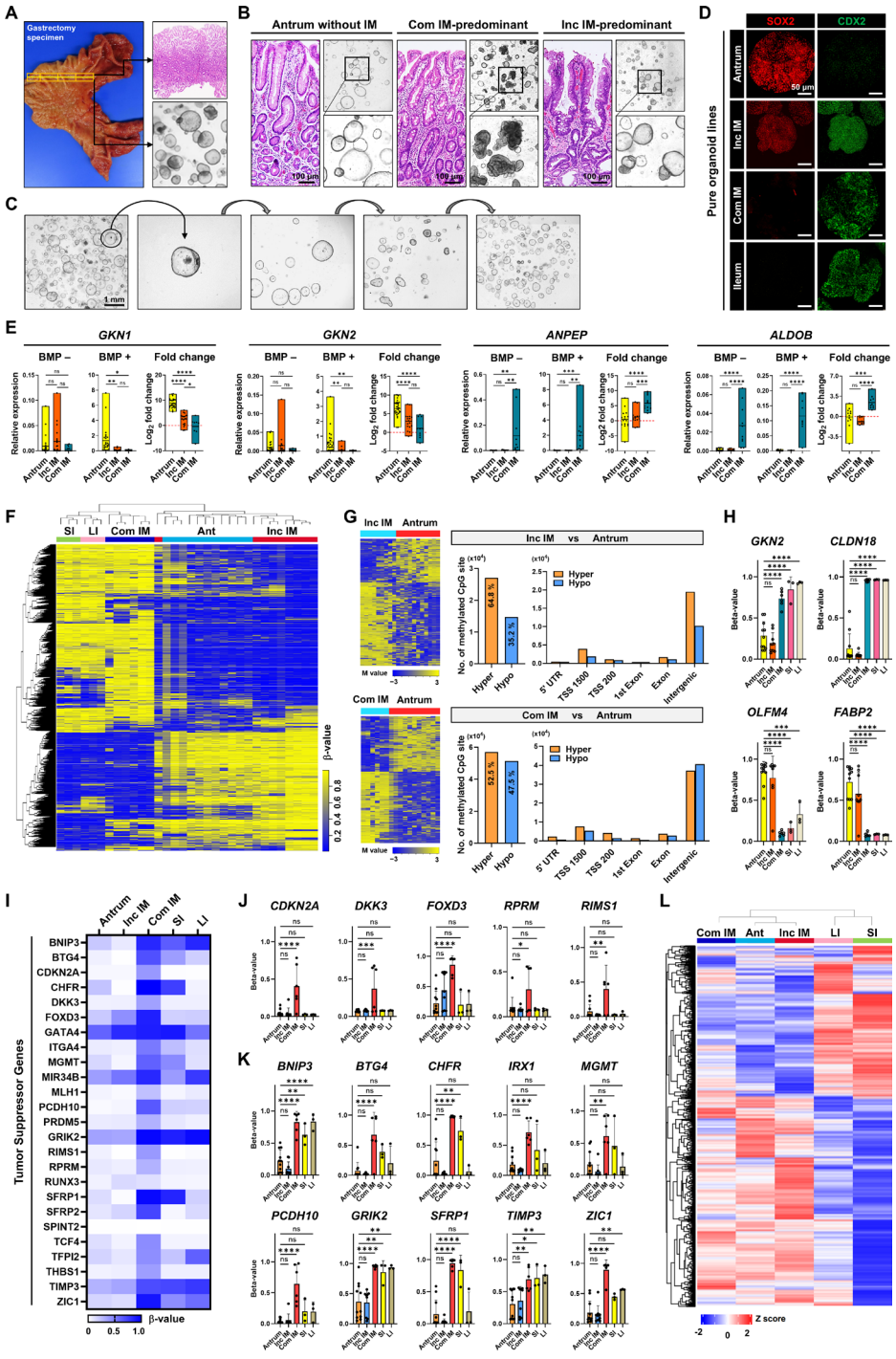

Figure 4 Generation of subtype-specific metaplastic organoids and characterisation of their epigenetic landscapes. (A) Gastric mucosal strips from gastrectomy specimens were analysed for the proportion and subtype of gastric intestinal metaplasia (GIM), followed by organoid culture. (B) Representative H&E and bright-field images of primary gastric organoids. (C) Generation of subtype-specific organoid lines by manual single-sphere picking and subculturing. (D) Immunostaining of organoids with SOX2 and CDX2. (E) Quantitative PCR analysis of stomach-enriched (*GKN1* and *GKN2*) and intestine-enriched (*ANPEP* and *ALDOB*) genes in subtype-specific organoid lines derived from antrum (n=19), incomplete (Inc) IM (n=14) and complete (Com) IM (n=10), with or without BMP stimulation. Data represent mean±SD; statistical analysis by one-way ANOVA with Tukey's multiple comparisons. (F) Unsupervised clustering of 10 000 highly variable probes from DNA methylation arrays performed on organoids from antrum (n=11), small intestine (SI, n=3), large intestine (LI, n=3), Inc IM (n=10) and Com IM (n=6). (G) Differential DNA methylation analysis comparing Inc IM versus antrum or Com IM versus antrum. Heatmaps represent 500 randomly selected CpG sites. The central bar plots indicate the number of hypermethylated and hypomethylated CpG sites. Right bar plots show their genomic distribution. (H) Methylation beta values at stomach (*GKN2* and *CLDN18*)-enriched and intestine (*OLFM4* and *FABP2*)-enriched gene loci. Data represent mean±SD; statistical analysis by one-way ANOVA with Dunnett's multiple comparisons test. (I) Heatmap showing mean beta values of tumour suppressor genes across samples. (J, K) Methylation beta values of tumour suppressor genes selectively hypermethylated in Com IM (J) and genes hypermethylated both in Com IM and intestinal samples (K). (L) Hierarchical clustering of chromatin accessibility profiles based on 3000 randomly sampled significant ATAC-seq peaks in organoid lines. ns, not significant; *p<0.05, **p<0.01, ***p<0.001, ***p<0.0001. ANOVA, analysis of variance; BMP, bone morphogenic protein.

methylation status of known tumour suppressor genes (TSGs), often aberrantly methylated in GC.[24] Intriguingly, Com IM organoids, but not Inc IM, exhibited elevated promoter methylation across a majority of these TSGs (figure 4I–K). Several genes demonstrated high methylation levels uniquely in Com IM (figure 4J), while others displayed similar methylation patterns in both Com IM and intestinal tissues, suggesting that promoter methylation of specific TSGs may represent a feature of intestinal lineage reprogramming (figure 4K). To further characterise chromatin dynamics, we conducted Assay for Transposase-Accessible Chromatin with sequencing on the organoid lines. Inc IM clustered most closely with antral organoids, whereas Com IM showed intermediate features and clustered with both antrum and Inc IM (figure 4L). Unlike its methylation profile, Com IM did not cluster with SI or LI, suggesting that chromatin accessibility changes may lag behind during metaplastic transformation. Together, Inc IM exhibits global intergenic hypermethylation, while retaining gastric epigenetic features. Conversely, Com IM adopts a more intestinal-like methylation profile along with promoter hypermethylation in TSGs.

Single-cell transcriptomic profiling of GIM organoids on BMP-induced differentiation

To further examine the lineage identity of GIM and to evaluate how closely subtype-specific gastric organoids mimic their in vivo counterparts, we performed scRNA-seq before and after BMP stimulation. Following BMP treatment, all organoid types exhibited characteristic thickening of the epithelial spheres and structural crowding, indicative of phenotypic and cellular transitions (figure 5A,B). UMAP projection and DGE analyses revealed lineage relationships that somehow differed from those inferred via spatial transcriptomic analysis. With broader transcriptomic coverage, Inc IM appeared more closely related to the antrum and despite strong histological resemblance and similarities in intestine-specific gene expression and methylation profiles, Com IM did not overlap with SI (figure 5C,D). This suggests that the phenotypic conversion observed in metaplasia does not require global transcriptional reprogramming but may instead be driven by selective regulation of lineage-specific genes.

Com IM organoids responded robustly to BMP stimulation, displaying significant upregulation of intestine-enriched genes (figure 5E and online supplemental figure 9A–C). In contrast, Inc IM organoids exhibited a modest increase in stomach-specific genes and a relatively attenuated induction of intestine-specific genes (figure 5E,F). Among the gastric markers, *GKN1* and *GKN2* were markedly upregulated, while intestinal markers including *ALDOB*, *CDX2*, *CDH17* and *KRT20* also showed significant but less pronounced increases (figure 5E,F). This differential response underscores the mixed lineage identity and partial differentiation capacity of Inc IM organoids. Consistent with the previous report,[25] BMP signalling activation led to the downregulation of deep antral gland cell-associated genes, *MUC6* and *AQP5* (figure 5F) and stem/progenitor-associated markers (online supplemental figure 9D–F), indicating a shift away from a progenitor state towards luminal differentiation. Immunostaining confirmed coexpression of gastric (GKN1) and intestinal (REG4) markers in Inc IM organoids (figure 5G), and showed reduced expression of deep antral gland cell markers in BMP-treated antral organoids (figure 5H). Collectively, our data demonstrate that Inc IM maintains a transcriptional profile closely resembling gastric antrum, yet possesses the capacity to coexpress gastric and intestinal lineage markers on differentiation cues.

Cellular phenotypic association of Inc IM with GC

Asian Cancer Research Group defines GC into four molecular subtypes: MSI, microsatellite stable/epithelial–mesenchymal transition (MSS/EMT), MSS/TP53 negative (MSS/TP53$^-$) and MSS/TP53 positive (MSS/TP53$^+$). To investigate how Inc IM relates to GC and its molecular subtypes, we constructed an additional tissue microarray incorporating 21 GCs (figure 6A,B and online supplemental figure 10A, B). UMAP illustrated how each GC mapped in relation to normal stomach, intestines and GIM subtypes (figure 6C). Transcriptomic profiling revealed that many GCs coexpressed lineage-specific markers of the stomach, SI and LI (figure 6D), a pattern reminiscent of Inc IM. Projecting individual GCs onto the UMAP further revealed their phenotypic proximity to Inc IM (figure 6E). Of the 21 GCs, 17 shared cell populations with Inc IM, while four (GC1, GC5, GC8 and GC14) appeared unrelated to Inc IM phenotypes. Given the well-documented stem-like properties of GC, we examined the expression of stem/progenitor-related genes across normal mucosa, GIM and GC samples. GC exhibited elevated expression of *DMBT1*, *HMGB2*, *SOX9*, *OLFM4* and *STMN1* (figure 6F). Notably, *DMBT1* was the only gene consistently expressed in both GIM subtypes and GC (figure 6F,G). Under inflammatory conditions, *DMBT1* expression was induced in the antrum but not the corpus (figure 6G), potentially explaining the antral predilection of GIM. Protein-level validation confirmed elevated DMBT1 and STMN1 expression in GC samples (figure 6H).

To investigate the phenotypic relevance of Inc IM to GC in depth, we assessed cluster proportions of GC and performed UMAP, trajectory and weight-based similarity analyses. We defined 'weights' as the degree of transcriptional similarity between GC cells and epithelial clusters from the antrum and GIM subtypes. Integration of GC samples revealed new cell clusters not present in normal or GIM tissues, which we termed cancer-specific clusters (CSCs). Each tumour exhibited a distinct cellular makeup and varying degrees of association with Inc IM. For example, GC1 (MSI) was dominated by CSC1 (figure 7A–C), while the remaining MSI tumours showed highest similarity to Un IM, antrum and Inc IM, respectively (online supplemental figure 11A–C). GC6 (MSS/EMT) was enriched in ISC/progenitor cell cluster and was most closely aligned with Com IM (figure 7D–F). Conversely, GC5 was dominated by a colon stem/progenitor cell cluster (online supplemental figure 11D–F). GC12 (MSS/TP53$^-$) was composed primarily of Inc IM progenitor cells (figure 7G–I). Among EBV-positive tumours (GC8 and GC9), GC8 was predominantly composed of CSC2, whereas GC9 was enriched for Inc IM and ISC/progenitor populations (online supplemental figure 11G–I). GC21 (MSS/TP53$^+$) exhibited a dominant Inc IM basal cell phenotype (figure 7J–L), and most MSS/TP53$^+$ tumours were primarily associated with GIM except GC17, a diffuse-type (signet ring cell) carcinoma (online supplemental figure 11K–N).

Overall, GC samples displayed a higher proportion of Inc IM-associated cell types (figure 7M). Although the cohort size limited statistical power, Inc IM-related cell types were more frequently observed in MSS/TP53$^-$ and MSS/TP53$^+$ subtypes compared with MSI and MSS/EMT tumours (figure 7N,O). When categorising cases by dominant weights, 38% (8 of 21) of GCs were most closely associated with Inc IM, followed by antrum (24%), Un IM (19%) and Com IM (19%) (figure 7P). These findings indicate that in addition to Inc IM, both Un IM and Com IM cell types appear to be significantly associated with GCs; collectively, approximately three-quarters of the GCs analysed in this study are linked to GIM. In addition, to evaluate

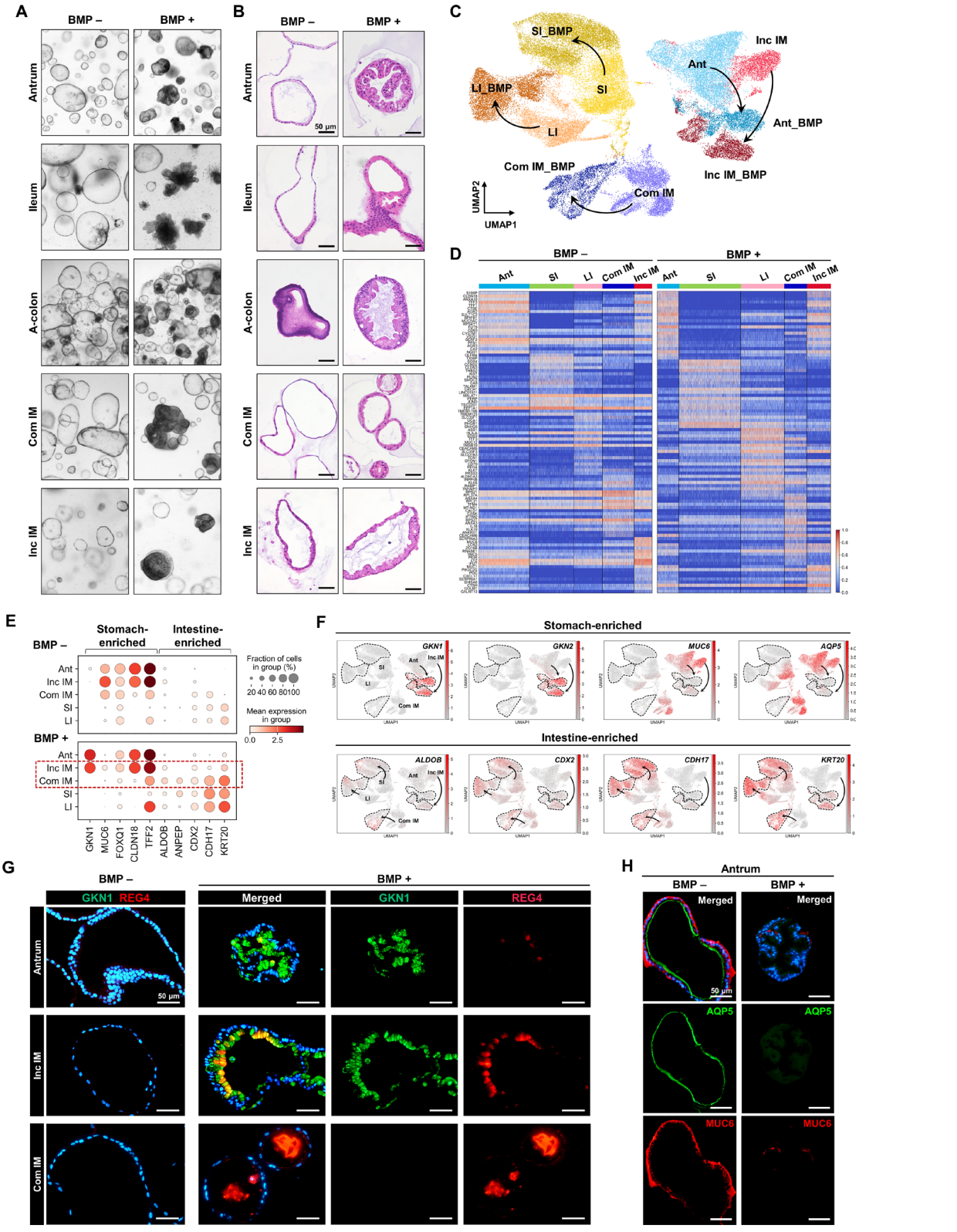

Figure 5 In vitro responses of subtype-specific metaplastic organoids to bone morphogenetic protein (BMP) signalling. (A, B) Representative bright-field (A) and H&E images (B) of subtype-specific organoids derived from the antrum, small intestine (SI), large intestine (LI), complete intestinal metaplasia (Com IM) and incomplete IM (Inc IM), cultured with or without BMP stimulation. (C) UMAP of single-cell RNA sequencing data from organoids before and after BMP treatment. The black arrows indicate the shift in cell populations following BMP stimulation. (D) Heatmap displaying differentially expressed genes before and after BMP treatment. (E) Dot plot showing changes in the expression of stomach-enriched and intestine-enriched genes following BMP stimulation. (F) Feature plots illustrating expression of stomach-enriched and intestine-enriched genes before and after BMP activation. Black arrows indicate the shift in cell populations following BMP stimulation. (G) Co-immunostaining with GKN1 and REG4 in the normal antrum and GIM organoids before and after BMP stimulation. (H) Co-immunostaining with AQP5 and MUC6 in the antral organoids before and after BMP stimulation. GIM, gastric intestinal metaplasia; UMAP, Uniform Manifold Approximation and Projection.

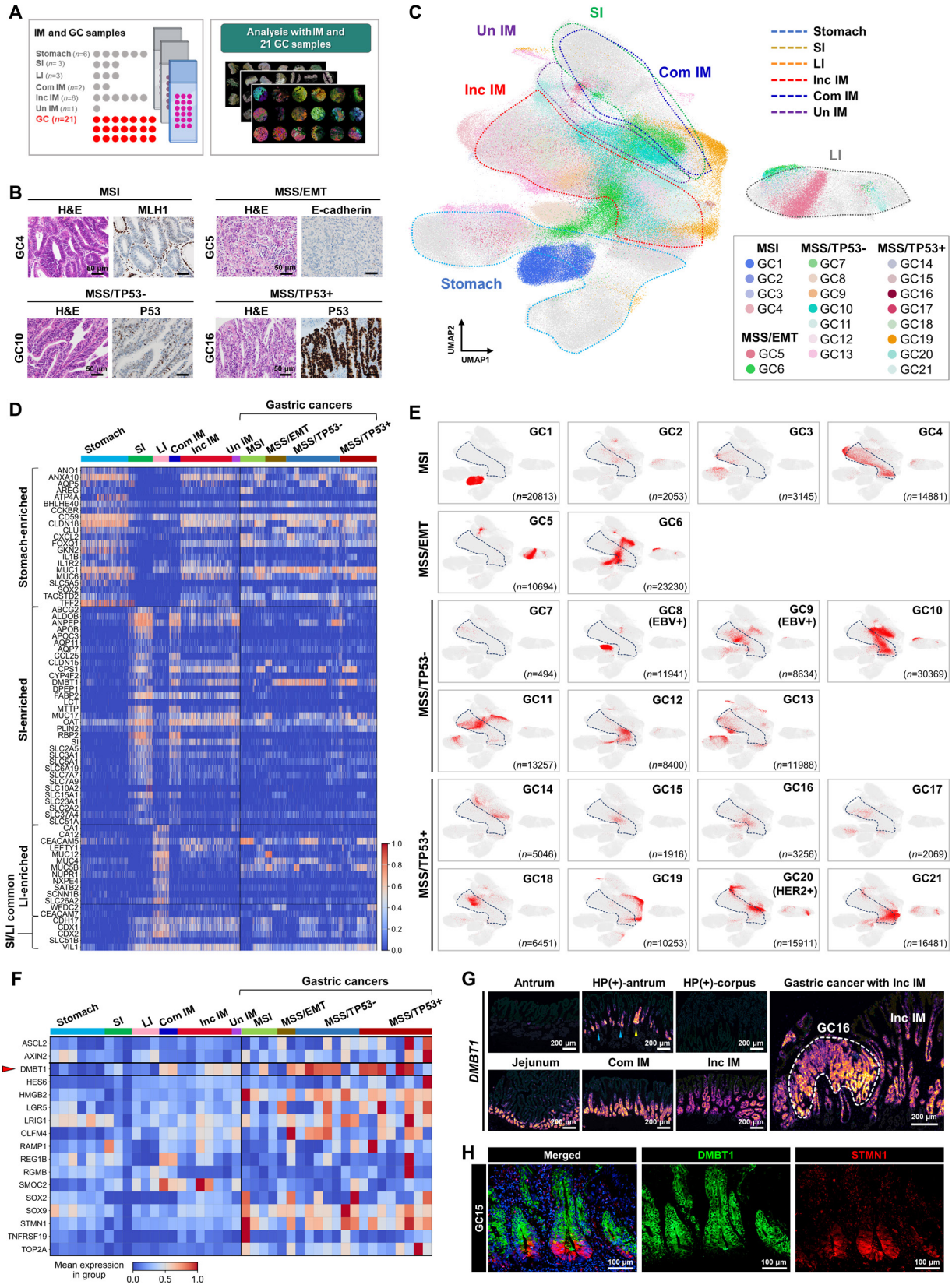

Figure 6 Cellular heterogeneity of gastric cancers (GC) and links to incomplete intestinal metaplasia (Inc IM). (A) Overview of spatial transcriptomic analysis conducted on normal gastric tissues (n=12), gastric IM (GIM; n=9) and (GC; n=21) samples. (B) Representative H&E and immunostaining images illustrating the four molecular subtypes of GC. (C) Integrated UMAP projection of all GC samples. Each cancer is colour-coded. (D) Heatmap showing lineage-enriched gene expression profiles across samples. (E) Individual UMAP plots for each GC sample, with cancer cell counts indicated. (F) Heatmap showing the expression of stem/progenitor cell-enriched genes across samples. Red arrowhead denotes *DMBT1*, a gene prominently expressed in both Inc IM and GC. (G) Xenium images showing *DMBT1* transcript localisation. (H) Co-immunostaining of a GC showing coexpression of DMBT1 and STMN1. LI, large intestine; SI, small intestine; UMAP, Uniform Manifold Approximation and Projection.

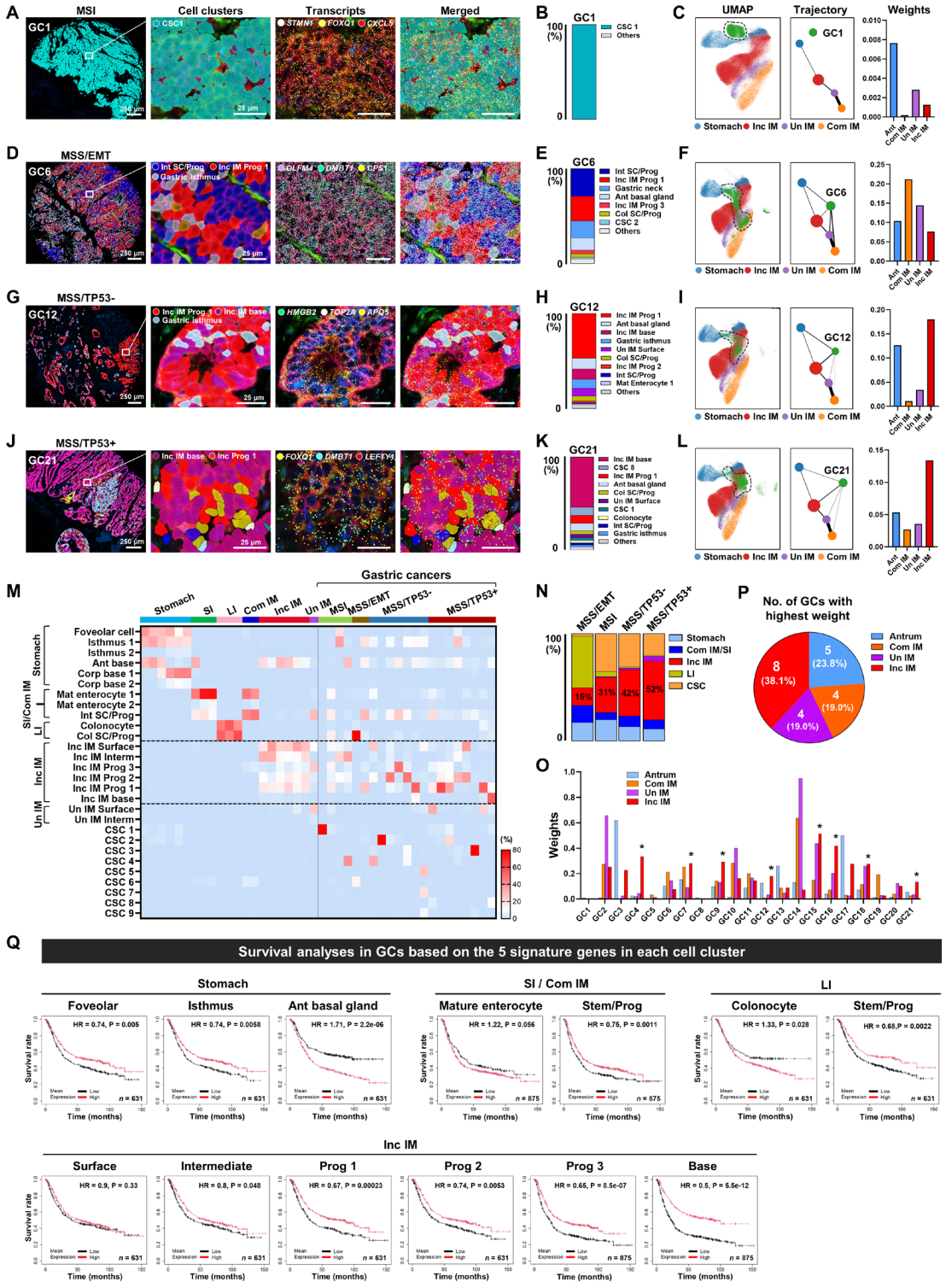

Figure 7 Enrichment of incomplete intestinal metaplasia (Inc IM)-associated cell types in gastric cancers (GC) and its prognostic implications. (A) Xenium images of GC1 showing cell cluster annotations and expression of indicated genes. (B) Bar graph showing the proportions of annotated cell clusters comprising GC1. (C) UMAP, lineage trajectory and similarity weights of GC1 to reference tissue types. (D) Xenium images of GC6 showing cell clusters and expression of indicated genes. (E) Bar graph showing cell cluster composition of GC6. (F) UMAP and lineage trajectory plots of GC6 with weights to reference tissue types. (G) Xenium images of GC12 with annotated clusters. (H) Bar graph depicting cluster composition of GC12. (I) UMAP and lineage trajectory plots of GC12 along with reference similarity weights. (J) Xenium images of GC21 showing cell cluster and expression of indicated genes. (K) Proportions of annotated clusters in GC21. (L) UMAP and lineage trajectory plots of GC21 with corresponding similarity weights. (M) Heatmap summarising the proportions of annotated cell clusters across samples. (N) Proportions of aggregated cell clusters categorised as stomach-, Com IM/small intestine (SI), Inc IM, large intestine (LI) and CSC-like cell types across GCs stratified by molecular subtype. (O) Bar graph displaying similarity weights of each GC to reference tissue types. Asterisks denote GCs with highest similarity to Inc IM. (P) Number of GCs with highest weights assigned to each reference type. (Q) Kaplan-Meier survival analysis of GC patients stratified by mean expression of five signature genes representing each cell type. CSC, cancer-specific cluster; UMAP, Uniform Manifold Approximation and Projection.

the prognostic significance of cellular phenotypes in GCs, we performed survival analyses using a large GC cohort.[26] DGEs for each cell type were derived from spatial transcriptomic data, and the top five DGEs per cell type were used to define signature gene sets (online supplemental table 6). Kaplan-Meier analysis revealed distinct survival patterns associated with specific cellular phenotypes (figure 7Q). Interestingly, Inc IM-related cell types did not correlate with poor prognosis. In particular, GCs dominated by Inc IM base cells demonstrated a significantly favourable prognosis. This is in line with the observations that intestinal-type GCs generally have more favourable outcomes.[27 28] Collectively, these results provide compelling evidence that a substantial subset of GCs may originate from Inc IM, potentially explaining the higher risk of GC observed in patients with Inc IM compared with those with Com IM.

DISCUSSION

Although scRNA-seq of human gastric tissues has significantly advanced our understanding of the genetic landscape of GIM,[12 13 29 30] it remains limited in its ability to distinguish between GIM subtypes. By leveraging spatial transcriptomics, we were able to dissect the molecular characteristics of each GIM subtype independently and identify distinct cell populations unique to Inc IM. This high-resolution approach allowed the analysis of both superficial differentiated cells and basal stem/progenitor populations within metaplastic glands. As expected, Com IM displayed a gene expression profile closely resembling that of the SI, consistent with its more differentiated and uniform intestinal phenotype, while Inc IM exhibited a hybrid transcriptomic signature incorporating features of gastric, SI and LI lineages. Notably, this mixed lineage profile was evident in both differentiated surface cells and basal stem/progenitor compartments of Inc IM, suggesting that the atypical phenotype of Inc IM may originate from multipotent progenitor cells with the capacity to adopt divergent epithelial fates. This parallels observations in Barrett's oesophagus, where metaplastic glands can follow a gastric line of differentiation giving rise to glandular diversity associated with dysplasia progression.[31] Our data offer a compelling explanation for the histological ambiguity and structural heterogeneity characteristic of Inc IM and also support the notion that Inc IM represents a metaplastic state that has failed to fully transition to a terminal intestinal phenotype, instead remaining in an intermediate phase between gastric and intestinal lineages.[32]

While several studies have reported the generation of GIM organoids,[33–35] it remains unclear whether they contain heterogeneous populations or which GIM subtypes they represent. To address this limitation, we developed subtype-specific metaplastic organoid lines. The establishment of these well-characterised, subtype-specific organoid lines representing Com IM and Inc IM provides a powerful platform for elucidating the genetic, epigenetic and phenotypic features unique to each metaplastic subtype. Moreover, they offer a valuable system for investigating the plasticity and potential interconversion between Com IM and Inc IM, further advancing our understanding of GIM heterogeneity.

By leveraging subtype-specific GIM organoids, we delineated distinct epigenetic landscapes underlying Com and Inc IM, respectively. DNA hypermethylation is a well-recognised molecular hallmark of GIM.[10] Recent genome-wide methylation profiling of highly purified GIM crypts has revealed widespread hypermethylation, identifying an IM-specific epigenetic signature that is also detectable in a subset of GC.[28] Our subtype-specific analysis revealed that Inc IM exhibits more extensive DNA hypermethylation than Com IM, primarily attributable to increased methylation at intergenic regions. In contrast, promoter hypermethylation of TSGs was confined to Com IM. Although the global methylation levels in Inc IM approached those of the SI, its overall methylation pattern remained more similar to that of antrum. Conversely, Com IM, despite exhibiting lower absolute methylation levels than both Inc IM and SI, displayed a methylation profile more closely aligned with SI, consistent with its more differentiated intestinal phenotype. These findings suggest that the success of intestinal lineage commitment during metaplasia is not solely dictated by the extent of DNA methylation but rather by locus-specific epigenetic reprogramming. While promoter hypermethylation of TSGs is a well-characterised driver of carcinogenesis, the functional implications of intergenic hypermethylation remain less well defined. Intergenic regions are enriched with enhancers and emerging evidence supports a regulatory role for methylation at these sites in modulating gene expression and influencing neoplastic progression.[36 37] Our observation of pronounced intergenic hypermethylation in Inc IM raises the possibility that this epigenetic alteration may contribute to the elevated cancer risk associated with this subtype. However, further mechanistic studies are warranted to elucidate its potential role in gastric carcinogenesis.

Spasmolytic polypeptide-expressing metaplasia (SPEM) lineage cells within a pyloric gland metaplasia, another form of gastric metaplasia that develops in the corpus, are widely recognised as precursors to GC, with their underlying molecular mechanisms being increasingly delineated through murine models.[38–42] Supporting its relevance in human disease, Kumagai *et al* recently reported a case in which SPEM, gastric adenoma and gastric adenocarcinoma lesions all shared an identical *KRAS* mutation, suggesting a clonal origin from a founder SPEM lineage.[43] In contrast, the role of GIM as a true precursor to GC remains less well defined. Many studies have sought to elucidate molecular links between GIM and GC.[10 11 43–48] For instance, Gutierrez-Gonzalez *et al* described a case in which GIM adjacent to a dysplastic gastric lesion harboured identical mutations in the TSGs *APC* and *TP53*.[47] Furthermore, large-scale cohort analyses by Huang *et al* identified genetic and epigenetic changes in GIM samples that may aid in stratifying patients by GC risk.[10 11] Despite these findings, no study to date has demonstrated a consistent presence of canonical oncogenic mutations in GIM at the population level. This is consistent with the simple view that GIM represents a non-neoplastic, predysplastic condition that precedes the acquisition of significant genetic alterations. Given the limitations of purely genetic analyses in resolving the cellular origin of GC, we propose that phenotypic profiling based on lineage differentiation status may offer a complementary and potentially more informative approach. Through the application of organ-specific gene expression profiling, we identified that a substantial subset of GCs harbours cell populations transcriptionally similar to those of Inc IM. The representation of Inc IM-like cells in these tumours was markedly higher than that of either Com IM or antrum cell types. These findings are supported by recent work from Yue *et al*, which demonstrated strong transcriptomic concordance between cell populations within GC and those derived from GIM organoids.[34] In addition, Hoft *et al* have identified a metaplastic subtype resembling Inc IM, arising from HP infection and autoimmune gastritis, which shared transcriptional features with GC.[49] While not definitive proof of a direct precursor–product relationship, the phenotypic convergence between Inc IM and GC cells suggests that a subset of GCs may originate from Inc IM.

Our study has several limitations that warrant consideration. First, the gene panel used was limited to approximately 300 targets, which may have introduced selection bias during cell clustering and reduced our ability to capture the full transcriptomic complexity of the GIM. Recently released technologies now offer expanded gene coverage, which will likely overcome this constraint in future studies. Second, the Xenium platform relies on an in situ hybridisation-based methodology, which, although highly specific and spatially resolved, presents challenges in detecting highly expressed genes due to optical crowding. This limitation can result in signal spillover, whereby transcripts from highly expressing cells are erroneously detected in neighbouring, non-expressing cells. Consequently, certain rare and specialised cell populations such as Paneth cells, enteroendocrine cells and tuft cells were not reliably identified in our dataset. Third, we included one case classified as an indeterminate form of GIM ('Un IM'), which exhibited overlapping morphological features of complete and incomplete subtypes. Although not an established pathological category, such ambiguous presentations are commonly encountered in clinical practice and reflect the recognised histological and molecular continuum of GIM. We believe inclusion of this case underscores the need for more objective criteria to define intermediate forms, which should be systematically validated in larger cohorts. Lastly, the number of GC cases included in our study was insufficient to achieve statistical significance for some observed associations with GIM subtypes. Nevertheless, we identified consistent and biologically meaningful trends that warrant further investigation in larger cohorts.

In summary, our findings define Inc IM as a distinct metaplastic phenotype marked by mixed gastric and intestinal lineage characteristics and a unique epigenetic landscape. The frequent presence of Inc IM-like cell populations in GCs strongly supports its identity as a high-risk precursor lesion. The establishment of subtype-specific Inc IM organoids offers a robust and physiologically relevant model for dissecting the molecular mechanism underlying GIM and its progression towards malignancy.

Author affiliations
[1]Department of Covergence Biomedical Science, Jeju National University College of Medicine and Graduate School of Medicine, Jeju-si, Korea (the Republic of)
[2]Autonomous Driving Decision Technology Vanguard Team, Hyundai Motor Company, Seoul, Korea (the Republic of)
[3]Department of Surgery, Jeju National University College of Medicine and Graduate School of Medicine, Jeju-si, Korea (the Republic of)
[4]Department of Surgery, Jeju National University Hospital, Jeju-si, Korea (the Republic of)
[5]Department of Pathology, Jeju National University College of Medicine and Graduate School of Medicine, Jeju-si, Korea (the Republic of)
[6]Department of Pathology, Hanyang University College of Medicine, Seongdong-gu, Korea (the Republic of)
[7]Department of Pathology, Hanyang University Medical Center, Seongdong-gu, Korea (the Republic of)
[8]Epithelial Biology Center, Vanderbilt University Medical Center, Nashville, Tennessee, USA
[9]Department of Surgery, Vanderbilt University Medical Center, Nashville, Tennessee, USA
[10]Department of Cell and Developmental Biology, Vanderbilt University, Nashville, TN, USA
[11]Nashville VA Medical Center, Nashville, TN, USA
[12]Department of Pathology, Jeju National University Hospital, Jeju-si, Korea (the Republic of)

Correction notice This article has been corrected since it published Online First. The author name, James R Goldenring, has been corrected.

Acknowledgements We extend our special thanks to JunLab Studio for their expert visualisation of Xenium and single-cell RNA sequencing (scRNA-seq) data, which significantly enhanced the interpretation of our findings. We also acknowledge the technical support provided by Superbiochip, Rocket Genomics, Geninus and Macrogen. We thank Jaechang Hyeon for his technical support to generate paraffin blocks and unstained slides of human gastric organoids. Additionally, we thank Professor Eui Tae Kim (KLVS) for providing access to the EVOS M7000 imaging system, which facilitated high-quality organoid data.

Contributors HK and BJ designed the study. HK, BJ, EP, MY and SY developed the methodology. BJ, HK and JK conducted software implementation and data curation. HK and BJ validated the results and performed formal analysis. BJ, JG and EC conducted the investigation. BJ, JM, IHJ and DL provided resources. HK and BJ wrote the original draft, and all authors contributed to the review and editing of the manuscript. HK, BJ and JK were responsible for visualisation. HK and BJ supervised the project and are the guarantors of this work, taking full responsibility for the overall integrity and conduct of the study.

Funding This research was supported by a grant from the MD-Ph.D/Medical Scientist Training Programme through the Korea Health Industry Development Institute (KHIDI), funded by the Ministry of Health & Welfare (RS-2024-0043937, to BJ); the Yuhan Innovation Programme (YIP) of Yuhan Corporation (YIP-2024, to BJ) and a grant from the National Research Foundation of Korea (NRF), funded by the Ministry of Science and ICT (MSIT) (RS-2023-NR076434, to HK), Republic of Korea.

Competing interests None declared.

Patient and public involvement Patients and/or the public were not involved in the design, or conduct, or reporting, or dissemination plans of this research.

Patient consent for publication Not applicable.

Ethics approval This study was approved by the Institutional Review Board of JNUH (IRB No. 2022-01-009). Participants provided informed consent before taking part in the study.

Provenance and peer review Not commissioned; externally peer reviewed.

Data availability statement Data are available on reasonable request. The raw and processed sequencing data generated in this study have been deposited in the Gene Expression Omnibus (GEO) under accession numbers GSE294729, GSE295640 and GSE295401. This includes scRNA-seq, Xenium, bulk ATAC-seq and DNA methylation microarray data.

ORCID iDs
Eunyoung Choi http://orcid.org/0000-0002-1501-1568
James R Goldenring http://orcid.org/0000-0002-7833-2940
Bogun Jang http://orcid.org/0000-0003-4683-8338

REFERENCES

1 Altayar O, Davitkov P, Shah SC, *et al*. AGA Technical Review on Gastric Intestinal Metaplasia-Epidemiology and Risk Factors. *Gastroenterology* 2020;158:732–44.
2 Giroux V, Rustgi AK. Metaplasia: tissue injury adaptation and a precursor to the dysplasia-cancer sequence. *Nat Rev Cancer* 2017;17:594–604.
3 Correa P, Piazuelo BM, Wilson KT. Pathology of Gastric Intestinal Metaplasia: Clinical Implications. *American Journal of Gastroenterology* 2010;105:493–8.
4 Matsukura N, Suzuki K, Kawachi T, *et al*. Distribution of marker enzymes and mucin in intestinal metaplasia in human stomach and relation to complete and incomplete types of intestinal metaplasia to minute gastric carcinomas. *J Natl Cancer Inst* 1980;65:231–40.
5 Segura DI, Montero C. Histochemical characterization of different types of intestinal metaplasia in gastric mucosa. *Cancer* 1983;52:498–503.
6 Tatematsu M, Tsukamoto T, Inada K. Stem cells and gastric cancer: role of gastric and intestinal mixed intestinal metaplasia. *Cancer Sci* 2003;94:135–41.
7 Otsuka T, Tsukamoto T, Mizoshita T, *et al*. Coexistence of gastric- and intestinal-type endocrine cells in gastric and intestinal mixed intestinal metaplasia of the human stomach. *Pathol Int* 2005;55:170–9.
8 Tsukamoto T, Mizoshita T, Tatematsu M. Gastric-and-intestinal mixed-type intestinal metaplasia: aberrant expression of transcription factors and stem cell intestinalization. *Gastric Cancer* 2006;9:156–66.

9 Gawron AJ, Shah SC, Altayar O, *et al*. AGA Technical Review on Gastric Intestinal Metaplasia—Natural History and Clinical Outcomes. *Gastroenterology* 2020;158:705–31.
10 Huang KK, Ramnarayanan K, Zhu F, *et al*. Genomic and Epigenomic Profiling of High-Risk Intestinal Metaplasia Reveals Molecular Determinants of Progression to Gastric Cancer. *Cancer Cell* 2018;33:137–50.
11 Huang KK, Ma H, Chong RHH, *et al*. Spatiotemporal genomic profiling of intestinal metaplasia reveals clonal dynamics of gastric cancer progression. *Cancer Cell* 2023;41:2019–37.
12 Tsubosaka A, Komura D, Kakiuchi M, *et al*. Stomach encyclopedia: Combined single-cell and spatial transcriptomics reveal cell diversity and homeostatic regulation of human stomach. *Cell Rep* 2023;42:113236.
13 Nowicki-Osuch K, Zhuang L, Cheung TS, *et al*. Single-Cell RNA Sequencing Unifies Developmental Programs of Esophageal and Gastric Intestinal Metaplasia. *Cancer Discov* 2023;13:1346–63.
14 Hayakawa Y, Nakagawa H, Rustgi AK, *et al*. Stem cells and origins of cancer in the upper gastrointestinal tract. *Cell Stem Cell* 2021;28:1343–61.
15 Silberg DG, Sullivan J, Kang E, *et al*. Cdx2 ectopic expression induces gastric intestinal metaplasia in transgenic mice. *Gastroenterology* 2002;122:689–96.
16 Mutoh H, Sakurai S, Satoh K, *et al*. Cdx1 induced intestinal metaplasia in the transgenic mouse stomach: comparative study with Cdx2 transgenic mice. *Gut* 2004;53:1416–23.
17 Graham DY, Zou WY. Guilt by association: intestinal metaplasia does not progress to gastric cancer. *Curr Opin Gastroenterol* 2018;34:458–64.
18 Tan SH, Swathi Y, Tan S, *et al*. AQP5 enriches for stem cells and cancer origins in the distal stomach. *Nature New Biol* 2020;578:437–43.
19 Sousa JF, Ham A-J, Whitwell C, *et al*. Proteomic profiling of paraffin-embedded samples identifies metaplasia-specific and early-stage gastric cancer biomarkers. *Am J Pathol* 2012;181:1560–72.
20 Sugano K, Moss SF, Kuipers EJ. Gastric Intestinal Metaplasia: Real Culprit or Innocent Bystander as a Precancerous Condition for Gastric Cancer? *Gastroenterology* 2023;165:1352–66.
21 Jang B, Lee S-H, Dovirak I, *et al*. CEACAM5 and TROP2 define metaplastic and dysplastic transitions in human antral gastric precancerous lesions and tumors. *Gastric Cancer* 2024;27:263–74.
22 Zhang Y, Que J. BMP Signaling in Development, Stem Cells, and Diseases of the Gastrointestinal Tract. *Annu Rev Physiol* 2020;82:251–73.
23 Kim H, Jang B, Zhang C, *et al*. Targeting Stem Cells and Dysplastic Features With Dual MEK/ERK and STAT3 Suppression in Gastric Carcinogenesis. *Gastroenterology* 2024;166:117–31.
24 Padmanabhan N, Ushijima T, Tan P. How to stomach an epigenetic insult: the gastric cancer epigenome. *Nat Rev Gastroenterol Hepatol* 2017;14:467–78.
25 Kapalczynska M, Lin M, Maertzdorf J, *et al*. BMP feed-forward loop promotes terminal differentiation in gastric glands and is interrupted by H. pylori-driven inflammation. *Nat Commun* 2022;13:1577.
26 Győrffy B. Integrated analysis of public datasets for the discovery and validation of survival-associated genes in solid tumors. *Innovation (Camb)* 2024;5:100625.
27 Fuchs CS, Mayer RJ. Gastric carcinoma. *N Engl J Med* 1995;333:32–41.
28 Takeuchi C, Yamashita S, Liu Y-Y, *et al*. Precancerous nature of intestinal metaplasia with increased chance of conversion and accelerated DNA methylation. *Gut* 2024;73:255–67.
29 Zhang P, Yang M, Zhang Y, *et al*. Dissecting the Single-Cell Transcriptome Network Underlying Gastric Premalignant Lesions and Early Gastric Cancer. *Cell Rep* 2019;27:1934–47.
30 Kim J, Park C, Kim KH, *et al*. Single-cell analysis of gastric pre-cancerous and cancer lesions reveals cell lineage diversity and intratumoral heterogeneity. *NPJ Precis Oncol* 2022;6:9.
31 Evans JA, Carlotti E, Lin M-L, *et al*. Clonal Transitions and Phenotypic Evolution in Barrett's Esophagus. *Gastroenterology* 2022;162:1197–209.
32 Goldenring JR, Mills JC. Cellular Plasticity, Reprogramming, and Regeneration: Metaplasia in the Stomach and Beyond. *Gastroenterology* 2022;162:415–30.
33 Nanki K, Toshimitsu K, Takano A, *et al*. Divergent Routes toward Wnt and R-spondin Niche Independency during Human Gastric Carcinogenesis. *Cell* 2018;174:856–69.
34 Yue SSK, Tong Y, Siu HC, *et al*. Divergent lineage trajectories and genetic landscapes in human gastric intestinal metaplasia organoids associated with early neoplastic progression. *Gut* 2025;74:522–38.
35 Mommersteeg MC, Simovic I, Yu B, *et al*. Autophagy mediates ER stress and inflammation in *Helicobacter pylori*-related gastric cancer. *Gut Microbes* 2022;14:2015238.
36 Bhasin JM, Lee BH, Matkin L, *et al*. Methylome-wide Sequencing Detects DNA Hypermethylation Distinguishing Indolent from Aggressive Prostate Cancer. *Cell Rep* 2015;13:2135–46.
37 Almamun M, Kholod O, Stuckel AJ, *et al*. Inferring a role for methylation of intergenic DNA in the regulation of genes aberrantly expressed in precursor B-cell acute lymphoblastic leukemia. *Leuk Lymphoma* 2017;58:2156–64.
38 Goldenring JR, Nam KT, Wang TC, *et al*. Spasmolytic polypeptide-expressing metaplasia and intestinal metaplasia: time for reevaluation of metaplasias and the origins of gastric cancer. *Gastroenterology* 2010;138:2207–10.
39 Choi E, Hendley AM, Bailey JM, *et al*. Expression of Activated Ras in Gastric Chief Cells of Mice Leads to the Full Spectrum of Metaplastic Lineage Transitions. *Gastroenterology* 2016;150:918–30.
40 Sáenz JB, Mills JC. Acid and the basis for cellular plasticity and reprogramming in gastric repair and cancer. *Nat Rev Gastroenterol Hepatol* 2018;15:257–73.
41 Brown JW, Cho CJ, Mills JC. Paligenosis: Cellular Remodeling During Tissue Repair. *Annu Rev Physiol* 2022;84:461–83.
42 Caldwell B, Meyer AR, Weis JA, *et al*. Chief cell plasticity is the origin of metaplasia following acute injury in the stomach mucosa. *Gut* 2022;71:1068–77.
43 Kumagai K, Shimizu T, Nikaido M, *et al*. On the origin of gastric tumours: analysis of a case with intramucosal gastric carcinoma and oxyntic gland adenoma. *J Pathol* 2023;259:362–8.
44 Correa P, Shiao YH. Phenotypic and genotypic events in gastric carcinogenesis. *Cancer Res* 1994;54:1941s–3s.
45 Fenoglio-Preiser CM, Wang J, Stemmermann GN, *et al*. TP53 and gastric carcinoma: a review. *Hum Mutat* 2003;21:258–70.
46 Gong C, Mera R, Bravo JC, *et al*. KRAS mutations predict progression of preneoplastic gastric lesions. *Cancer Epidemiol Biomarkers Prev* 1999;8:167–71.
47 Gutierrez-Gonzalez L, Graham TA, Rodriguez-Justo M, *et al*. The clonal origins of dysplasia from intestinal metaplasia in the human stomach. *Gastroenterology* 2011;140:1251–60.
48 Kumagai K, Shimizu T, Takai A, *et al*. Expansion of Gastric Intestinal Metaplasia with Copy Number Aberrations Contributes to Field Cancerization. *Cancer Res* 2022;82:1712–23.
49 Hoft SG, Brennan M, Carrero JA, *et al*. Unveiling Cancer-Related Metaplastic Cells in Both Helicobacter pylori Infection and Autoimmune Gastritis. *Gastroenterology* 2025;168:53–67.